Evolution of selfish multicellularity

collective organisation of individual spatio-temporal regulatory strategies

Renske M.A. Vroomans[*,1,3], Enrico Sandro Colizzi[2,3]

Affiliations

[*] Corresponding author: renske.vroomans@slcu.cam.ac.uk

[1] Origins Center, Netherlands; Informatics Institute, University of Amsterdam

[2] Origins Center, Netherlands; Mathematical Institute, Leiden University

[3] Sainsbury Laboratory, University of Cambridge

Abstract

Recent studies have shown that many major signalling pathways involved in embryonic development are ancient, and likely evolved before or at the onset of multicellularity. In the unicellular ancestors, these pathways may have been involved in regulating their ecological interactions. To understand the early evolution of development, we therefore need to study how the ancestral genetic toolkit was co-opted to coordinate nascent multicellularity in this ecology-to-development transition.

We construct an evolutionary cell-based model in which cells use their genetic toolkit to compete for resources in a spatially structured environment. First, we let unicellular ancestors evolve a genetic toolkit that enables them to survive by regulating their behaviour in response to the environment. Then, when adhesion can evolve, we find that adhering groups of cells interpret environmental cues more effectively than their unicellular ancestors, which enables them to locate resources more quickly – this selects for multicellularity. Once cells have evolved multicellularity, their genetic toolkit evolves to a drastically different strategy from the unicellular ancestor, resulting in striking patterns of spatio-temporal cell state changes that visually resemble animal development. Surprisingly, these coordinated patterns are not a consequence of cells cooperating with each other. Rather, they result from cells using their genetic toolkit to compete with other cells in the cluster, selfishly maximising their own reproductive success.

Our model demonstrates how emergent selection pressures at the onset of multicellularity can drive the evolution of the ecological interactions between cells to give rise to developmental pattern formation.

Introduction

The evolution of multicellularity is a major transition in individuality, which occurred multiple times across the tree of life [1–3]. These transitions were likely driven by an initial increase

in cell-cell adhesion [4] - as also shown by *in vitro* evolution experiments [5, 6], leading to cluster formation by aggregation or by inhibition of cell separation [3, 7–9]. The unicellular ancestors of these nascent multicellular organisms exhibited complex behaviour and were capable of switching to different phenotypes in response to changes in the environment [10]. When adhesion evolved, the newly multicellular aggregates consisted of complex cells that could exploit their pre-existing genetic toolkit to this new biotic environment.

In fact, many of the genes necessary for coordinating multicellular development, including adhesion proteins, transcription factors and signalling genes, were already partially present in the unicellular ancestor and extant closely related unicellular species [8, 9, 11–14]. This suggests that the genetic toolkit used by the unicellular ancestor to regulate cell behaviour, may have formed the basis for stable cell differentiation and division of labour in multicellular clusters [3, 15, 16]. The evolution of multicellular development therefore involved protein domain shuffling, expansion of existing gene families and rewiring of gene interaction networks, more than *de novo* evolution of genes [12–14]. Only after the transition would the progressive complexification of multicellular development have led to the large expansion of the transcription factor families, distal enhancers and other complex regulatory mechanisms [4, 14]. Here, we construct a computational model that includes evolvable unicellular genetic toolkits, to recapitulate the first steps of this evolutionary transition - from the ecology of unicellular populations to the development of multicellular organisms.

The evolution of cell differentiation at the onset of multicellularity has been studied in computational models from the perspective of division of labour (usually between soma and germ line), where trade-offs between costs and benefits of functional specialisation and multicellularity determine the size of clusters [17–20]. These models assume the existence of multiple stable cell states, and find the selective conditions under which both states arise in a group of cells. Alternatively, multicellular life-cycles can arise spontaneously because of conflicts between social groups of cells [21], or because of the interactions between cells' internal regulation and a changing environment [22]. Group-level selection emerging in spatially structured models can drive the evolution of differentiation, resulting in proto-developmental dynamics [23] and genome structuring [24]. Spatial differentiation patterns and cell-cell communication can also naturally arise as a mean to stabilise intracellular gene regulation [25], or as a by-product of selection for different cell-types [26]. However, it is still unclear how the regulatory program of the unicellular ancestors gave rise to the developmental program of multicellular organisms.

We have previously shown that adhesion can evolve in response to an emergent selection pressure for collective migration [27]. Here, we investigate how the regulatory program of independent, unicellular organisms changes in reaction to the evolution of adhering clusters. We use a multi-scale computational model of an evolving population of spatially embedded cells that have to find resources to survive. Cells have evolvable adhesion proteins and an evolvable regulatory network which determines their behaviour in response to a seasonally changing environment. Through their regulatory network and by sensing their environment, cells decide when

to divide, and when to migrate towards the resources, allowing for various survival strategies that are characterised by one or multiple phenotypic switches between these two states.

We find that in an environment with high selection pressure, cells evolve one of two strategies, depending on whether adhesion can co-evolve. When adhesion cannot evolve, competition between cells is dominated by reaching the resources first – they have to navigate the abiotic environment to find the resources by themselves. When adhesion can evolve, cells can perform collective migration. This lowers the pressure to reach resources quickly, because cells carry each other to the peak of the gradient [27]. Competition between cells then becomes driven by ensuring more division. This maximization of individual's reproductive success in the multicellular group shows that selection on cell behaviour becomes dominated by the newly established biotic environment. Thus, even within the simple context of our model, we observe a complex evolutionary transient that involves intricate feedback between cooperation and competition. The interactions between cells within clusters, and between cells and the environment, lead to an emergent coordination of migration and division which strongly resembles morphogenesis.

Results

Model setup

We model an evolving population of cells that have to locate resources necessary for survival in a periodically changing environment, throughout multiple seasons. We implement a 2D hybrid Cellular Potts Model (CPM) for the cellular dynamics, using a square lattice for the cells and a lattice of the same dimensions for a chemoattractant signal (Fig. 1A). [27–30]. Cells can adhere to each other based on the ligands and receptors that they express on their membrane (Fig. 1A). The greater the complementarity between the ligands and receptors of two cells that are in contact, the stronger their adhesion. This is translated to the cell-cell and cell-medium adhesion energy in the CPM (respectively $J_{\mathrm{c,c}}$ and $J_{\mathrm{c,m}}$, see Methods). In some simulations, the receptors and ligands can evolve, thereby changing the strength of adhesion or repulsion between cells. In simulations where adhesion cannot evolve, we set $J_{\mathrm{c,c}}$ and $J_{\mathrm{c,m}}$ such that the surface tension γ between cells and the medium is negative. This means that cells preferentially interact with the medium, and thus do not adhere to each other.

Cells can be in one of two states: migratory or dividing, which are mutually exclusive phenotypes in our model (due to conflicting use of the cytoskeleton). When the *in silico* cells are migratory, they perform a persistent random walk and chemotaxis towards higher local concentrations of the chemoattractant signal (Fig. 1A). The chemoattractant is deposited as a gradient with a peak on one side of the lattice; this gradient is steep enough that cells are able to migrate to the peak individually. The location of the peak changes to a random side of the lattice (up, down, left or right) at the start of each new season. Dividing cells are stationary and also do not react to the chemoattractant. When cells have been in the "dividing" state continuously for 10000 CPM update steps (Monte Carlo Steps, MCS – see Methods), they slowly start increasing

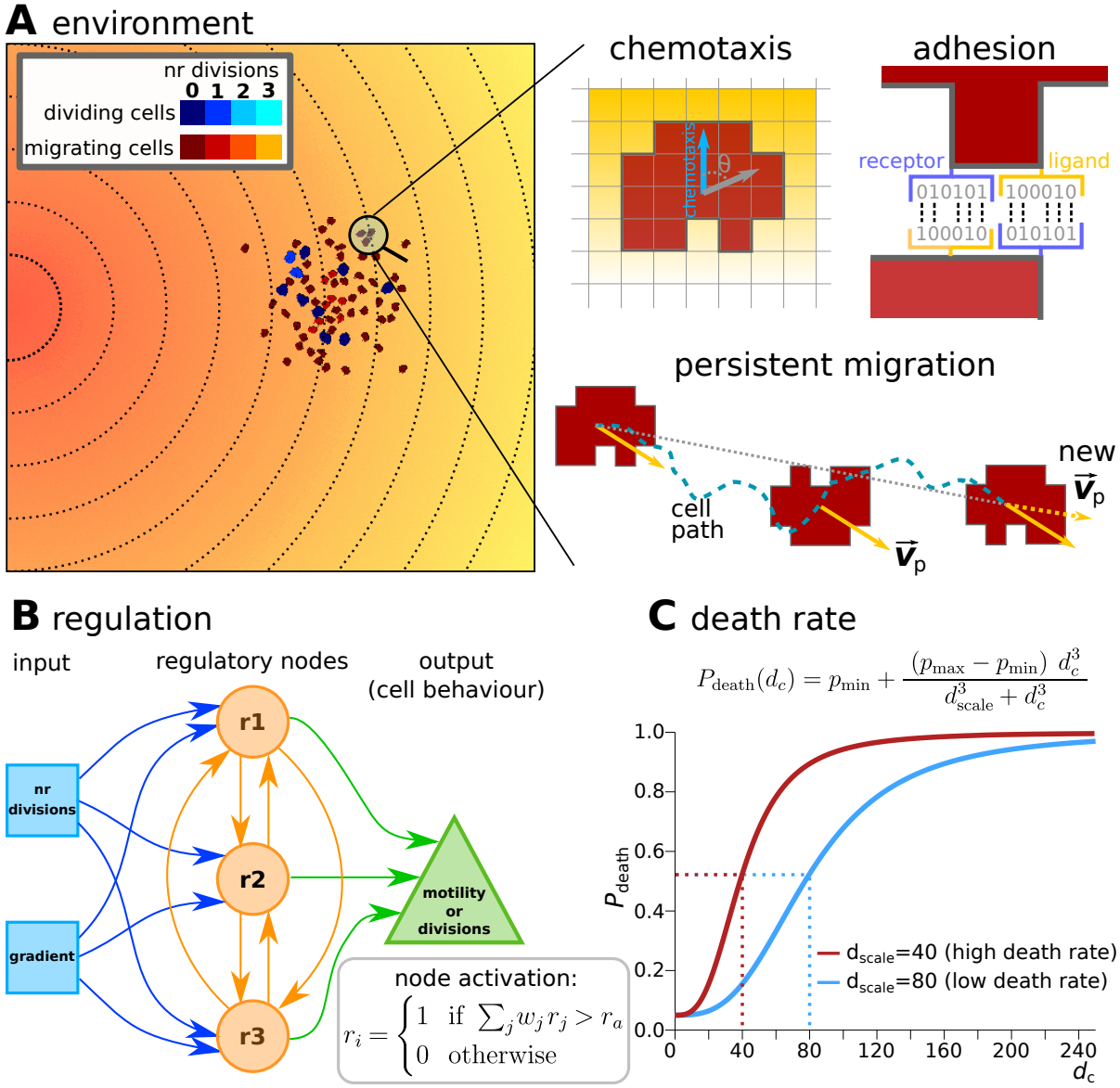

Figure 1: Model description. a) The environment in which cells have to survive contains a chemoattractant gradient (lines and colour indicate equal amounts of chemoattractant). Cells can sense the chemoattractant in the lattice sites that correspond to their own location, and move preferentially in the direction of perceived higher concentration (the blue arrow). Adhesion between two cells is mediated by receptors and ligands (represented by a bitstring, see [26]). The receptor of one cell is matched to the ligand of the other cell and vice versa. The more complementary the receptors and ligands are, the lower the J values and the stronger the adhesion between the cells. Persistent migration is implemented by endowing each cell with a preferred direction of motion $\vec{v}_p$. Every τ_p MCS, this direction is updated with a cell's actual direction of motion in that period. **b)** Cells have a simple evolvable regulatory network to determine whether to migrate or divide at any given time (with max 3 divisions). The network receives as input the number of divisions the cell has already done, and the concentration of the gradient. The activation threshold (r_a) and strength of interaction (w_j) between nodes can evolve. **c)** Probability for a cell to die at the end of a season, as a function of its distance to the peak d_c (in lattice sites). d_{scale} determines the distance at which the probability is half-maximal.

their size over another 20000 MCS. When they have grown to twice the size, they perform a division. Each cell can divide a maximum of three times during each season, implicitly assuming that resources acquired by a cell are finite, and a cell's available energy is capped.

The state of a cell is determined by an evolvable gene regulatory network (GRN), modeled as a Boolean network with a fixed architecture, loosely based on [31] (Fig. 1B). The network receives two inputs: the average local concentration of the chemoattractant at the cell's location, and the number of times the cell has already divided. It has three regulatory genes that process the input and determine the state of the output gene, which determines cell state: migratory or dividing (see Methods). When a cell has performed the maximum number of divisions in a season, it cannot divide anymore even when the state of its output gene dictates a dividing state. Instead, the cell is in a quiescent state in which it is neither dividing nor migrating. When a cell divides, the daughter cell inherits the receptors and ligands for adhesion and the GRN architecture; the state of all genes in the networks of both cells is reset to 0. In one of the daughter cells, mutations can happen in the strength of the gene regulatory interactions in the GRN and in the activation threshold of each gene.

Each season, cells have a fixed amount of time to divide and migrate. Cells that are closer to the peak of the gradient at the end of the season have a higher probability to survive into the next season than cells that are further away (Fig. 1C). At the start of each new season, the division counter in each cell, and the states of the genes in their GRN, are reset to 0.

Evolved regulatory strategies depend on death rate, season length and adhesion

We assessed the effect of season duration, seasonal death rate and evolution of adhesion on the evolution of cells' regulatory strategy. We ran 15 simulations for each combination of season duration (short, intermediate or long), seasonal death rate (low or high), and the possibility of evolving adhesion, as summarised in Table 1. Each simulation was initialised with a starting population of cells possessing random GRNs, which could evolve over subsequent seasons. For milder conditions (lower death rates and longer seasons), populations in all 15 simulations could evolve viable strategies, in which cells switch at least once between migration and dividing (Fig. 2A). This led to a large population capable of reaching the peak of the gradient before the end of the season. In the simulations with intermediate season duration, higher death rates causes some populations to go extinct because cells were unable to evolve such switching. Under the harshest conditions (high death rates and very short seasons), 4 to 7 of the populations went extinct (table 1).

Cells evolved several regulatory strategies, with different combinations of migration and division timing (Fig. 2A). These different strategies could be distinguished by the timing of their divisions: early in the season, late, or somewhere in between. When divisions happened early in the season (a "division-early strategy"), most cells performed all three divisions first and then

Table 1: Number of surviving populations (out of 15)

season length	death rate	No adhesion	adhesion
500000 MCS	low	15	15
	high	15	14
250000 MCS	low	15	15
	high	12	12
180000 MCS	low	13	14
	high	8	11

low: $d_{\text{scale}} = 80$; high: $d_{\text{scale}} = 40$

switched to the migratory state (Fig. 2A, top row; Supp. fig. S1B; Supp. Vid. 1,2). In ”division-late strategies”, cell behaviour more often depended on where the cell was located on the lattice. Cells typically migrated until they reached a particular concentration of the chemoattractant, performed a division, and then migrated further before dividing again at a higher chemoattractant concentration (Fig. 2A, bottom row; Supp. Fig. S1C; Supp. Vid. 3,4). Populations with a division-late strategy remained smaller compared to division-early strategies, because fewer cells completed all three divisions during the season (Supp. Fig. S2).

In simulations where adhesion could not evolve, we observed that a broad range of division timing strategies evolved when conditions were mild (Fig. 2C, top left; Season duration = 500000 MCS and death rate = 80). Simulations with shorter seasons (250000 or 180000 MCS) and higher death rate (40) led to progressively more “division late” solutions ((Fig. 2C, bottom left; Supp Fig. S3). In simulations where the the receptors and ligands for adhesion were allowed to evolve, the population rapidly became multicellular, regardless of season duration or death rate (Fig 2B). This is due to the increased efficiency of collective migration, and the competitive advantage of adhering cells at the peak of the gradient [27]. These simulations also yielded a broad range of division timing strategies when evolved under mild conditions (Fig 2 C, top right), but for harsher conditions we found that the evolved strategies display earlier divisions (Fig 2 C, bottom right). This suggests that the evolution of adhesion strongly affects the selection on regulatory strategy.

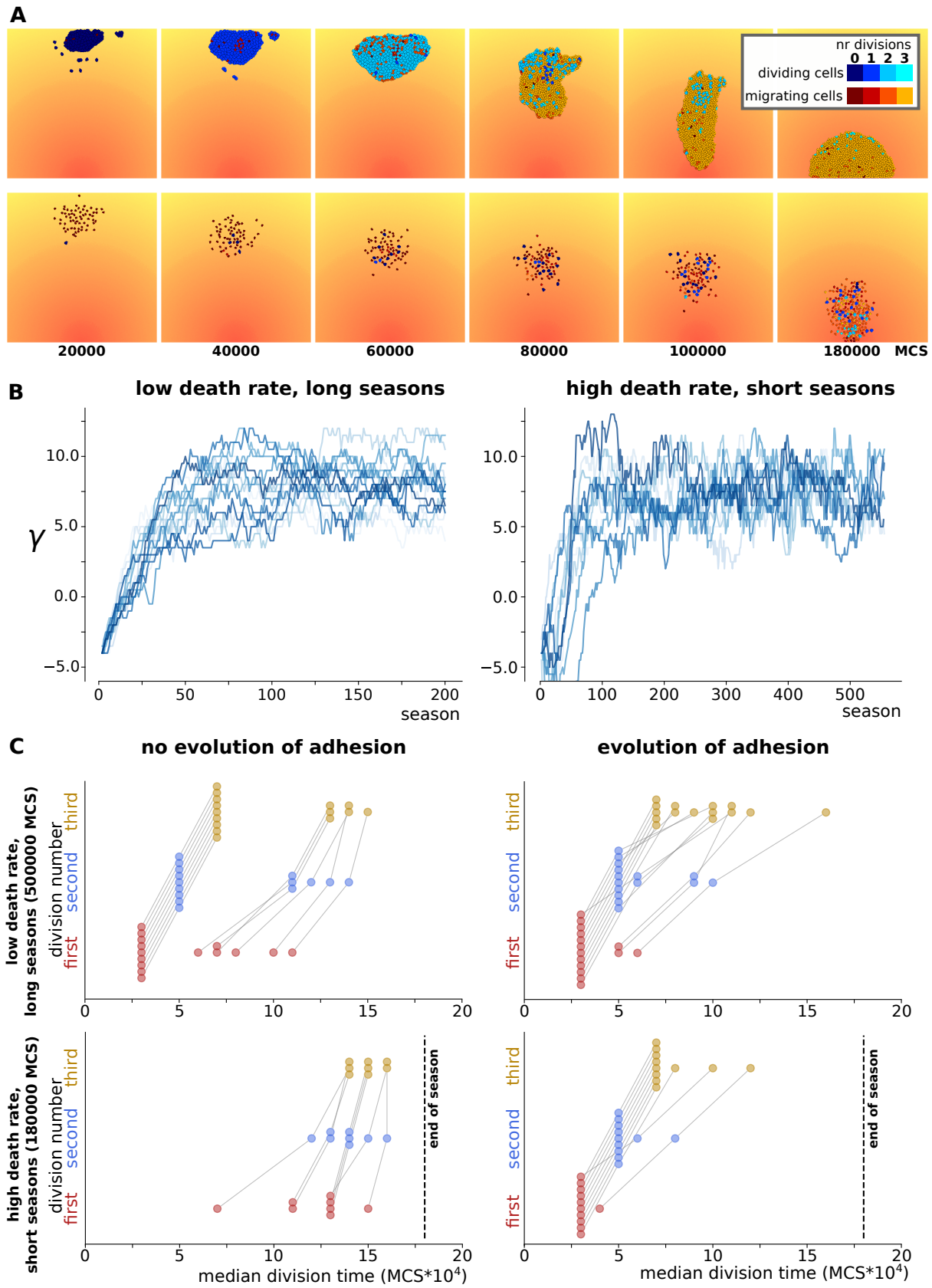

Figure 2: Evolved regulatory strategies differ in the timing of cell divisions a) Snapshots of the population over the course of one season, in two simulations where different regulatory strategies evolved; one with and one without evolution of adhesion (season length 180000 MCS). Colours denote the state of the cell (dividing=blue, migrating=red/yellow; lighter colours indicate larger number of cell divisions). **b)** Evolution of adhesion in 15 independent simulations with low death rate and long seasons, and in 15 simulations with high death rate and short seasons **c)** The median timing of cell divisions of the last 10 seasons in different sets of simulations. Lines between dots connect values belonging to the same simulations (see also Supp. Fig. S3).

Multicellular clusters evolve different regulatory strategies than unicellular organisms

Under harsh conditions, cell populations evolved different strategies depending on whether adhesion could evolve. We next assessed whether these strategies were evolutionarily stable under switched adhesion conditions. We selected 4 individuals from different high-death rate, short-season simulations that were evolved without adhesion and let them evolve their adhesion strength. 4 individuals evolved with adhesion were used for simulations without any adhesion (keeping their adhesion at negative γ). Each of these individuals was used to start a new population in 5 independent simulations.

The new populations which could mutate their ligands and receptors, first rapidly evolved strong adhesion (Supp. Fig. S4). Concurrently, they also evolved a division-early strategy, especially for their first division (Fig. 3A,B). Two factors contributed to earlier divisions: collective migration and the evolved regulation. Collective cell migration speeds up the group's chemotaxis compared to a single cell [27], allowing cells to reach the chemoattractant concentration at which they divide at an earlier time – particularly when cells have a division-late strategy (Supp. Fig. S5). Their gene regulation also evolved so that divisions occurred at a lower concentration of the chemoattractant gradient (Fig. 3C, Supp. Fig. S6A).

Instead, the individuals that were switched to simulations without adhesion gave rise to populations which evolved towards a division-late strategy Fig. 3A', B'). This was partly due to the difference in dynamics between adhering and non-adhering groups: nonadhering cells hinder each other while moving up the gradient, leading to a slight delay in reaching the signal to divide compared to single cells; however, this was mostly true for division-late individuals, and the effect was small (Supp. Fig. S5). The main cause for the evolution of later division times was a change in regulation: cells evolved to divide at a higher chemoattractant concentration (Fig. 3C'; Supp. Fig. S6B).

In summary, the evolutionary simulations show a clear change in regulatory strategy in reaction to a change in adhesion (Fig. 4). The speed of adaptation however depended on the ancestral strategy, with the division-late strategies typically being faster to change to a division-early strategy than vice versa (compare Fig. 3B with B').

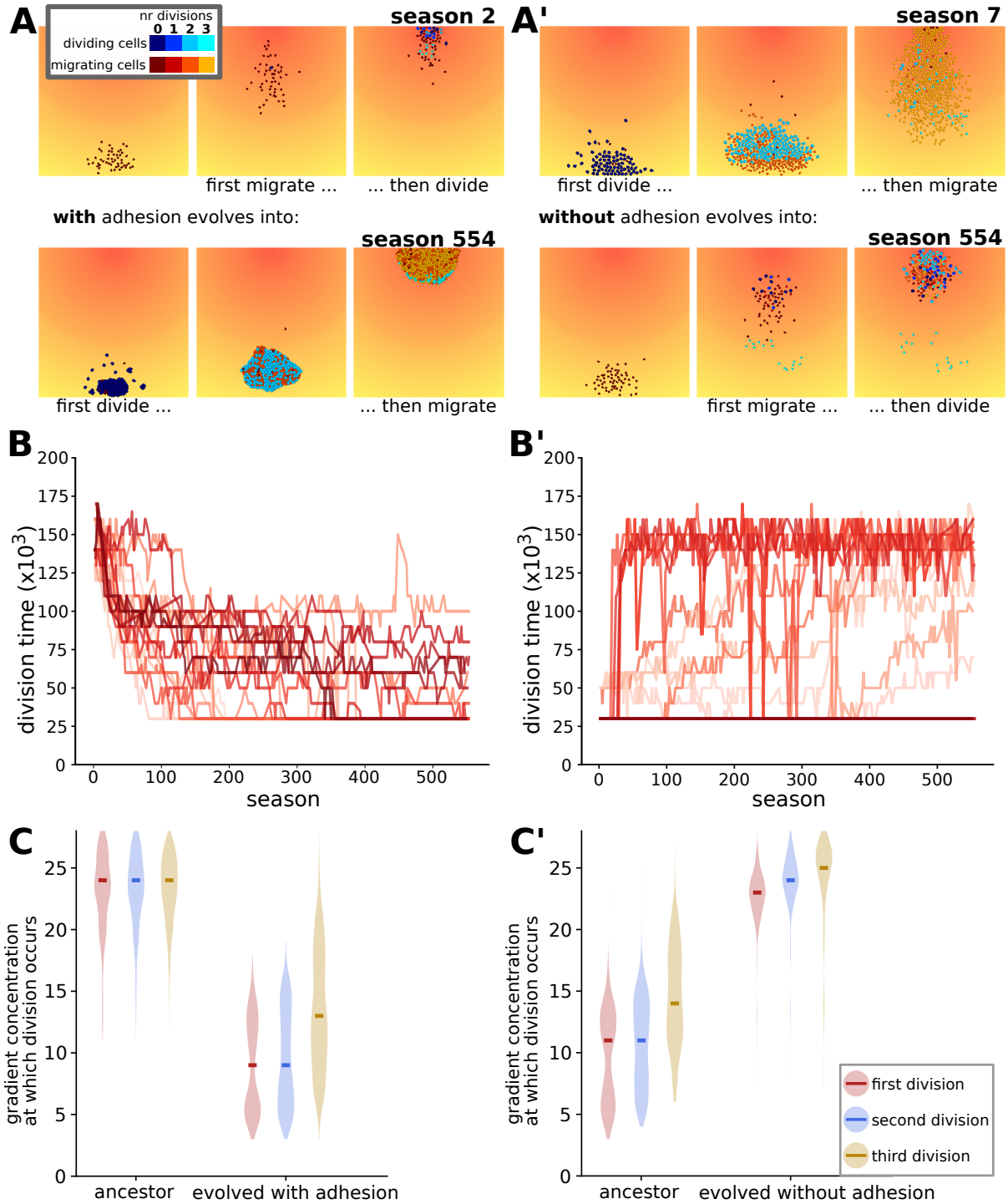

Figure 3: In absence of adhesion, populations evolve towards a division-late strategy.
a-a') Snapshots of a simulation from a simulation with a division-late (a) or a division-early (a') ancestor that evolved towards the opposite strategy due to a switch in adhesion possibility (a: switch from simulation without adhesion to simulation with adhesion; a' vice versa.) (seasons chosen where the peak is on the opposite side of the lattice). **b-b')** The evolution of the timing of the first division, for all simulations with switched adhesion. Median value of the population at any time point. Colour distinguishes the different simulations in one plot. **b)** bottom panel: evolution of adhesion strength (γ) in all simulations switched from no adhesion to evolution of adhesion. Higher γ indicates stronger adhesion. **c-c')** The concentration at which the three divisions occur, for an ancestor and descendant populations in 1 of the 5 replicate simulations. The thick lines indicate the median of the population. All other replicates can be found in Supp. Fig. S6.

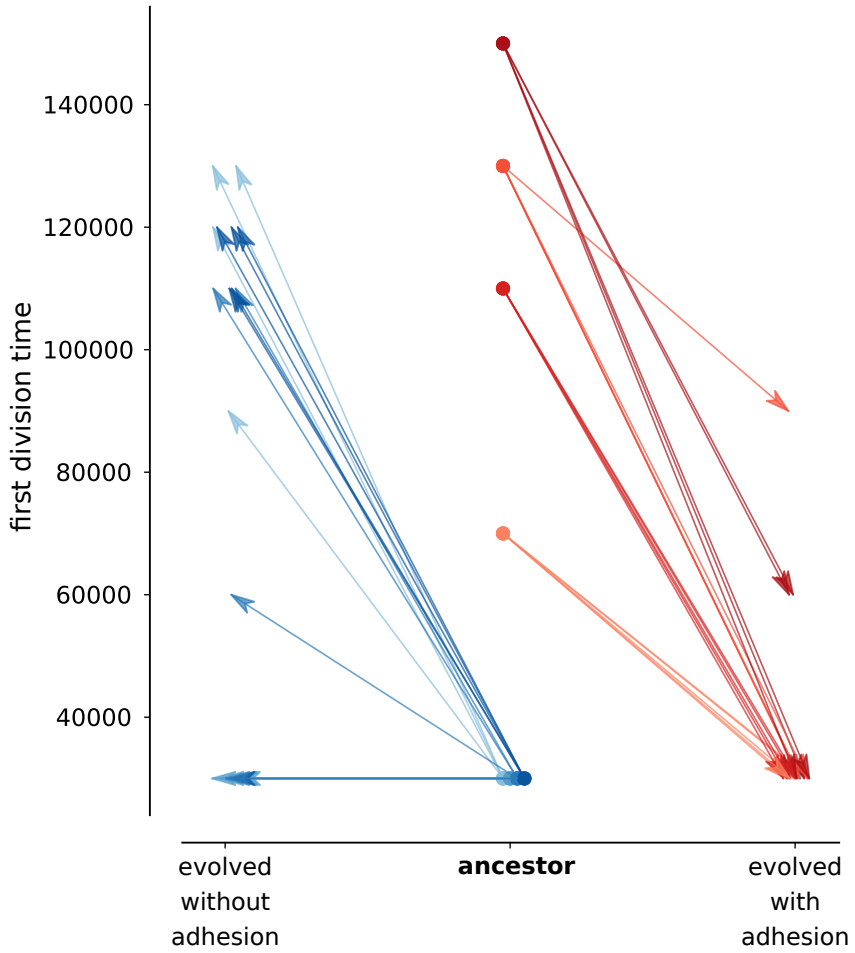

Figure 4: Summary of changes in division time in all simulations.
Average timing of the first cell division in the last ten seasons of the simulations, evolved either without cell adhesion or with the possibility of evolving adhesion. Center point indicates the ancestral strategy with which continued simulations were started. Four different ancestral strategies from simulations without adhesion were allowed to continue evolution with adhesion, and vice versa (5 independent simulations per ancestral strategy).

Presence of adhesion determines type of interference competition and selfish behaviour

We next set up competition experiments to investigate how emergent population dynamics cause a selective advantage for division-late strategies in unicellular populations, and for division-early strategies in multicellular groups. We placed two groups of cells with different strategies or different adhesion strengths next to each other at the end of the lattice opposite the peak of the gradient (Fig. 5A). Cells were allowed to migrate and divide, but no mutations could happen upon division, so that all cells in a group kept the same strategy. Cell death occurred at the end of each season as in the evolutionary simulations, and simulations were run until one of the groups went extinct.

When we let an adhering group compete with a non-adhering group with the same regulatory strategy, we found that adhering groups were closer to the peak at the end of each season, regardless of their strategy (Fig. 5B). We observed that adhering groups migrate slightly more efficiently, but mainly outcompete non-adhering cells at the peak, by excluding non-adhering cells (Fig. 5B and Supp. Vid. 5,6). The strong interference competition at the peak of the gradient explains why adhesion evolved rapidly in all evolutionary simulations. Then we let ancestral strategies compete with a descendant that evolved a different strategy under switched adhesion conditions.

We let a division-early ancestor compete with a descendant from an evolutionary run without adhesion, and assigned both groups a negative adhesion value ($\gamma_{c,m} = -4$). In this case, the cells with the descendant strategy were closer to the peak throughout each season (Fig. 5C). The division-late strategy won because non-adhering cells exclude each other from the peak. The cells that reached the peak sooner were locked in place by the pressure exercised by the later-arriving migratory cells. (Supp. Vid. 7). However, in the first season there were significantly fewer cells of the descendant group, indicating that this strategy sacrificed cell divisions to get to the peak sooner.

We then let a division-late ancestor compete with a descendant from a simulation with evolution of adhesion, assigning both groups a high adhesion value in the competition experiment ($\gamma_{c,m} = 6$). The competition dynamics of these two groups were more complex. The division-late ancestor reached the peak of the gradient earlier than its descendant. While the descendant reached the peak with a larger population size, both groups had the same population size at the end of the season. Because adhesion was mediated by identical ligands and receptors, the two groups mixed freely. However, when we plotted the distance of both groups over multiple seasons, we found that the ancestor had a harder time staying close to the peak towards the end of the season, despite arriving there earlier (Fig. 5E). The videos show that the ancestral cells were displaced because many still performed divisions close to the peak, and were therefore in a non-migratory state (Supp. Vid. 8).

In summary, when cells cannot evolve adhesion, their evolution is driven by a competition for reaching and occupying the peak first. This leads to a division-late strategy, where cells combine the use of the abiotic environmental cues (the gradient) with the information on their internal state. This strategy yields a survival benefit due to lower death rates, but at the cost of fewer divisions. When cells can (and do) evolve adhesion, they optimise the use of their biotic environment, i.e., the other cells. Adhesion allows cells to reduce competition at the peak of the gradient, and exploit each other for migration while maximising their divisions. Cells therefore become more selfish as adhesion – and thereby collective migration – evolves. The change in selection pressure as the cellular context changes is the hallmark of differentiated multicellular organisation. Finally, the multicellular clusters often displayed spatial patterns of cell differentiation that resembled development, with morphogenetic events such as stretching and compression of the multicellular cluster (think for instance of convergent extension [32,

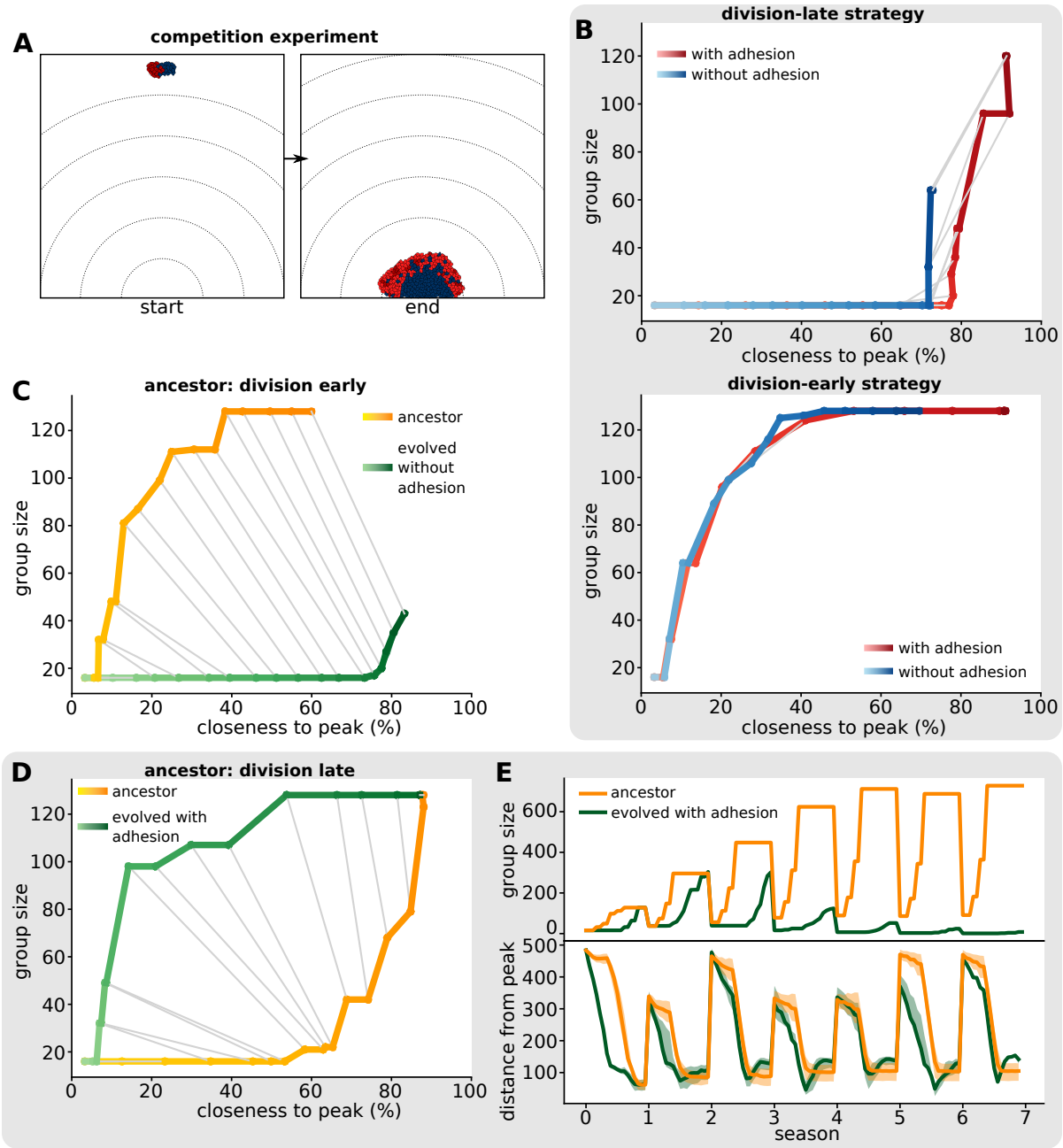

Figure 5: Competition experiments show that selective advantage depends on presence of adhesion.

a) Setup of competition experiment: two groups of each 16 cells are placed adjacent to each other, with differing regulatory networks or differing adhesion values. The simulation is then run for multiple season (without mutations), until one of the groups has gone extinct. **b-d)** Group size plotted against the median distance of cells to the peak of gradient, shown for the first season of the competition experiment (0%=maximum distance, 100%=at the peak). Grey lines connect equal time points. Colour gradient of the first line also indicates time passage. Replicates can be found in Supp. Fig. S7. **b)** Competition between two groups with the same regulatory strategy, one adhering ($\gamma = 6$), the other non-adhering ($\gamma = -4$). **c)** Competition between ancestral, division-early strategy and evolved, division-late strategy; both non-adhering. **d)** Competition between two adhering groups, one with an ancestral, division-late strategy and one with a strategy evolved after 500 seasons with possibility of adhesion (having become more division-early). **e)** Time dynamics of the competition in d. Top plot shows group sizes, bottom plot shows distance to the peak. Shading indicates 25th and 75th percentile of population.

33]). This is especially clear for the dynamics of a genetically homogeneous cluster (Fig. 6, Supp. Vid. 9).

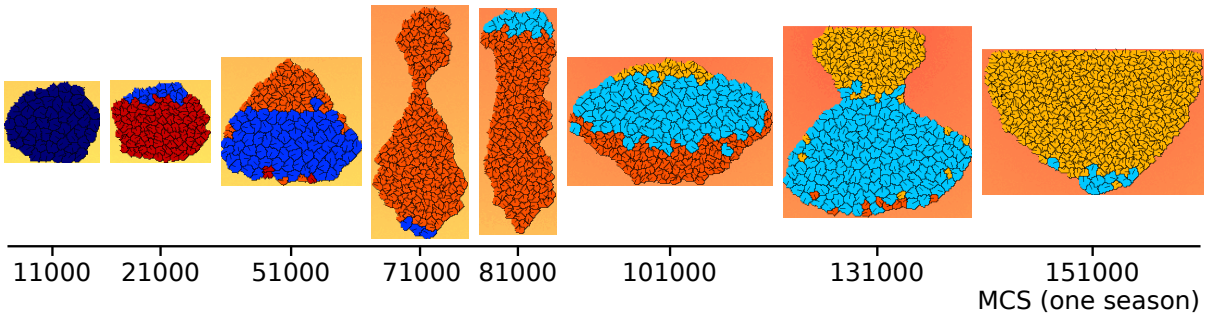

Figure 6: Development of genetically homogeneous cluster
Images of a developing cluster started with 50 genetically identical cells with a regulatory strategy taken from from a simulation evolved with adhesion (death rate = 80, season duration = 180000). Images are centered on the cluster.

Discussion

In this study, we show how the evolution of adhesion changes the competition dynamics between cells that are able to sense and react to their environment. In both the unicellular and the multicellular case, cells selfishly maximise their replication, but the evolved strategy to do so depends on the abiotic and cellular context. Cells' regulatory strategy evolves towards a division-late strategy when adhesion cannot evolve, because of competition to reach the resources necessary for survival. Adhesion facilitates collective migration and cell mixing, thereby lifting the selection pressure to reach the resources first. In this case, cells compete to perform all divisions while remaining in the migrating cluster, and to remain as close to the peak as possible by being in a migratory state there. Thus, the abiotic environment determines competition in absence of adhesion, while the biotic environment – the other cells – determines competition in the presence of adhesion. We therefore expect that at the transition to multicellularity, the regulatory program of unicellular organisms drastically changed its dynamics to suit the new (cellular) environment – yielding proto-developmental patterning as a side effect of the process.

Current bioinformatic evidence from the holozoan relatives of animals points to a unicellular ancestor that had a complex life cycle, possibly with a multicellular stage, and a significant regulatory toolkit [10]. Our results show that the ancestral toolkit could have enabled a rapid evolution of new strategies for competition within a newly multicellular context. We find that the temporal behaviour of cells, which results from their individual decoding of the environment, can already yield transient spatial patterning in the multicellular cluster. The pattern is further stabilized by the differential sorting between migrating and dividing cells. No large changes to the available genetic toolkit are required for such patterning, only refinements of the existing regulation.

Cell states are organised by a gradient produced by the embryo in complex multicellular organisms. In contrast, external and internal cues combine to generate pattern formation in simpler multicellular organisms. For instance, in the multicellular alga *Volvox carteri*, dark-light transitions govern the differentiation of cells into somatic and germline cells, depending on their size after embryogenesis [34]. Similarly, in the multicellular (slug) phase of the slime mould *Dictyostelium discoideum*'s life cycle, cells migrate up external gradients of heat and light, causing different cell types to sort into specific regions along the body of the slug [35, 36]. Environmental cues triggering multicellularity can also be biotic: bacterial molecules induce aggregation in the choanoflagellate *Algoriphagus machipongonensis* [37], while some myxobacteria [38] and slime moulds migrate collectively to feed on bacteria [39]. Previous models have highlighted the effect of motility on the evolution of adhesion in social [40, 41] and non-social groups [27]. Our current model suggests that the transition to multicellularity may be driven by collective migration and increased competition within the cell cluster, and that external gradients may have provided the cues for spatial pattern formation and cell differentiation. Experimental evolution with unicellular or transiently multicellular phototactic or chemotactic species may provide a test of these predictions.

We do not observe a complete temporal-to-spatial shift in these simulations, as has been hypothesized for the transition to multicellularity [42]. Cells keep switching between states to maximise their own growth and survival. We expect that multilevel competition between multiple distinct multicellular clusters may be required to select for stable differentiation, as division of labour between cells may result in more successful groups. Additionally, the evolution of stable patterning may require a more evolvable genetic toolkit, which can expand to facilitate more complex regulation of cell-state, adhesion and cell-cell signalling.

In our previous study [27], we found that adhesion can evolve in response to an emergent selection pressure for collective migration in a noisy environment. Here, we show that competition between cells also drives the evolution of differentiation patterns in emerging multicellular organisms, leading to selfish multicellularity.

Acknowledgements

We thank Bram Hoogland and Pjotr van der Jagt for their thorough reading of the draft and helpful suggestions. This research is partly supported by the Origins Center Netherlands (NWA startimpuls).

Methods

We model an evolving population of cells that can adhere to each other, divide, migrate and perform chemotaxis on a two-dimensional lattice containing a gradient of chemotactic signal. Cells consist of multiple lattice sites, giving them an explicit shape and volume. They also

contain an evolvable gene regulatory network that senses the environment and regulates the decision to either divide or migrate (explained below). Cell dynamics on the lattice (movement, adhesion) are governed by the Cellular Potts Model (CPM) formalism [28, 29] and simulated with a Monte Carlo method. The population undergoes a seasonal culling, in which cells further from the gradient source have a higher chance of dying. Then, the gradient source is placed at a different position, after which the new season starts. The custom software, written in C^{++}, can be found at [43].

Regulation of cell behaviour Cells have a simple evolvable regulatory network that determines their behaviour: either migrating and following chemotactic signals, or growing and dividing. The overall network architecture has been previously used to model gene regulation in micro-organisms [31]. The network receives as input the local concentration of chemoattractant (a real number between 0 and 28) and the number of times the cell has already divided. There are three regulatory nodes. The state of each regulatory node is determined by combining these two inputs with the state of the other two regulatory nodes. The output node takes as input the state of the regulatory nodes, to determine whether the cell is in a migratory or dividing state. The regulatory nodes and output node are Boolean. Their new states are calculated synchronously from the previous state, as follows:

$$r_i = \sum_j w_j S_j$$

$$S_i = \begin{cases} 1 & \text{if } r_i > r_a \\ 0 & \text{otherwise} \end{cases}$$

where S_i is the new state of node i. The new state is 1 if the value of the regulation is greater than its activation threshold r_a. When the node j is an input node, S_j is the value of the input node times an evolvable scaling factor f_j; otherwise it is the Boolean state of a regulatory node (including i itself). For each cell, the network state is updated every 20 MCS, to even out microscopic cell fluctuations. The networks of different cells are updated out of step to prevent artificial synchrony between cells.

When the state of the output node is 0, the cell is in migratory mode. When the state is 1 for η_{init} consecutive timesteps, the cell enters the dividing cell state, during which it does not migrate or perform chemotaxis. It will need η_{grow} timesteps to grow to twice the size (by increasing target size, A_T, every η_{grow}/A_T MCS) and prepare for division before it can actually divide. If, in that time, the output node becomes 0, the cell will shrink again and revert back to the migratory state, and will start the division process anew if the output node becomes 1 again. Once the cell divides, the state of all nodes is reset to 0. A cell can divide a maximum of three times per season; when the output node remains one after that, the cell is non-migratory, but won't divide again.

Upon cell division, the regulatory network is passed to the daughter cell with the possibility of mutations. Each parameter of the network (w, f, r_a) mutates independently during

cell division. Mutations occur with probability μ_ω and change the values taken from a normal distribution with mean 0 and $\sigma = 0.05$.

Cellular Potts Model The Cellular Potts Model dynamics are implemented with the Tissue Simulation Toolkit [30], on a regular square lattice $\Lambda_1 \subset \mathbb{Z}^2$ of size $L \times L$. A cell c consists of the set of lattice sites $\vec{x} \in \Lambda_1$ with the same spin s, i.e. $c(s) = \{\vec{x} \in \Lambda_1 \mid \sigma(\vec{x}) = s\}$. The chemotactic signal is located on a second plane Λ_2, of the same size and spacing as Λ_1.

The cells move in the Λ_1 lattice due to the displacement of their boundary, arising from stochastic fluctuations. These fluctuations tend to minimise a cell's energy, whose terms correspond to biophysically motivated cell properties ([44]). The Λ_1 lattice is updated through the Metropolis algorithm. Each Monte Carlo step (MCS), $L \times L$ lattice sites are drawn randomly. For each site belonging to the boundary of a cell, a random site from its Moore neighbourhood, $\vec{x}$, is selected which may copy its spin value $\sigma(\vec{x})$ into this lattice site. Whether an attempted spin copy is accepted depends on the contribution of several terms to the energy H of the system, described by the Hamiltonian, as well as other biases Y. A copy is always accepted if energy is dissipated, i.e. if $\Delta H + Y < 0$ (with $\Delta H = H_{\text{after copy}} - H_{\text{before copy}}$), and may be accepted if $\Delta H + Y \geq 0$ because of "thermal" fluctuations that follow a Boltzmann distribution:

$$P(\Delta H, Y) = e^{\frac{-(\Delta H + Y)}{T}}$$

with $T = 16$ the Boltzmann temperature (in Arbitrary Units of Energy AUE), which controls the probability of energetically unfavourable copy events. The Hamiltonian consists of two terms, corresponding to cell size maintenance and adhesion:

$$H = H_{\text{cell size}} + H_{\text{adhesion}}$$

The copy biases, or "work terms", Y consist of terms corresponding to cell migration and chemotaxis:

$$Y = Y_{\text{migration}} + Y_{\text{chemotaxis}}$$

Cell size maintenance Cell size $A(c) = |c(s)|$, the number of lattice sites that compose a cell, is assumed to remain close to a target size A_T. Deviations from the target size are inhibited by adding the following term to the Hamiltonian:

$$H_{\text{cell size}} = \sum_{c \in C} \lambda \left(A\left(c\right) - A_T\right)^2$$

with C the set of cells and λ representing the resistance of cells against volume changes. A cell's target volume may grow when it prepares to divide, and is halved again upon division (see also below).

Cell adhesion The total adhesion energy resulting from interfaces between cells and with the medium is implemented as:

$$H_{\text{adhesion}} = \sum_{(\vec{x},\vec{x}\,')} J\left(\sigma(\vec{x}), \sigma(\vec{x}\,')\right)\left(1 - \delta\left(\sigma(\vec{x}), \sigma(\vec{x}\,')\right)\right)$$

summing over all pairs of neighbouring pixels with different s: $(\vec{x}, \vec{x}\,')$. $\delta\left(\sigma(\vec{x}), \sigma(\vec{x}\,')\right)$ is the Kronecker delta which restricts the energy calculations to the interfaces.

As previously described [27], cells express ligand and receptor proteins on their surface that determine the surface energy of cell interfaces, $J\left(\sigma(\vec{x}), \sigma(\vec{x}\,')\right)$. Ligands and receptors are modelled as binary strings of fixed length ν (Fig. 1). Cell adhesion increases (i.e. lower J values) with greater complementarity between their receptors R and ligands I (i.e. larger Hamming distance $D(R, I) = \sum_{i=1}^{\nu} \delta(R_i, I_i)$). Thus, given two cells with spin values σ_1 and σ_2 and their corresponding pairs of receptors and ligands $(R(\sigma_1), I(\sigma_1))$ and $(R(\sigma_2), I(\sigma_2))$:

$$J\left(\sigma_1, \sigma_2\right) = J_\alpha + 2\nu - D(R(\sigma_1), I(\sigma_2)) - D(R(\sigma_2), I(\sigma_1))$$

with $J_\alpha = 4$ so that $J\left(\sigma_1, \sigma_2\right)$ ranges between $[4, 52]$.

Adhesion of a cell with medium is assumed to depend only on the cell (the medium is inert, i.e. $J\left(\sigma_{\text{medium}}, \sigma_{\text{medium}}\right) = 0$), and in particular it depends only on a subset of the ligand proteins of a cell. This subset consists of the substring of I which begins at the initial position of I and has length ν'. The value of $J\left(\sigma_1, \sigma_{\text{medium}}\right)$ is calculated as:

$$J\left(\sigma_1, \sigma_{\text{medium}}\right) = J'_\alpha + \sum_{i=1}^{\nu'} F(i) I_i$$

$$F(i) = \begin{cases} 4 & \text{if } i = 1 \\ 3 & \text{if } i = 2 \\ 2 & \text{if } i = 3 \\ 1 & \text{if } 4 \leq i \leq 6 \end{cases}$$

with $J'_\alpha = 8$ and $F(i)$ a piece-wise defined function (a lookup table). The J values range in the interval $[8, 20]$. The strength with which cells adhere to each other depends on both the J value between the cell and the medium, and the J value of the interaction between cells. This can be represented by the γ value, the surface tension between cells and medium:

$$\gamma = J_{\text{c,m}} - \frac{J_{\text{c,c}}}{2}$$

When γ is negative, cells preferentially interact with the medium and do not adhere. In simulations where adhesion cannot evolve, we set $J_{\text{c,c}} = 36$ and $J_{\text{c,m}} = 14 \rightarrow \gamma = -4$, yielding nonadhering cells.

In a subset of simulations, the bitstrings of the receptor and ligand responsible for adhesion are mutated upon cell division. These mutations occur in onle one of the two daughter cells (chosen at random) with a per-position probability $\mu_{\text{R,I}}$. Mutations flip individual bits (from 0 to 1, and vice versa).

Cell migration We model migration (following [45]) by biasing cell movement to their previous direction of motion $\vec{p}(c)$: extensions of a cell are energetically more favourable when they are closer to the direction of that cell's $\vec{p}$:

$$Y_{\text{migration}} = -\mu_{\text{p}} \cos(\theta_p)$$

Where μ_{p} is the maximum energy contribution due to migration, and θ_p is the angle between $\vec{p}$ and the vector that extends from the center of mass of the cell to the lattice site into which copying is attempted. Every τ_p MCS the vector $\vec{p}$ is updated to reflect the actual direction of displacement of the cell over the past τ_p MCS (scaled to unit) (Fig. 1). We set $\tau_p = 50$ MCS. Whether a cell migrates depends on its internal state. Dividing cells do not migrate, so their $\mu_{\text{p}} = 0$. Non-dividing cells have $\mu_{\text{p}} = 3$. Note that all cells have the same τ_p, but they update their vectors at different MCS to prevent them from moving synchronously.

Chemotaxis Individual cells are able to migrate towards the perceived direction of a chemoattractant gradient. In contrast to [27], the slope of the gradient is steeper and we removed a source of noise in the gradient signal, allowing individual cells to identify the location of the peak with ease.

The chemotactic signal is represented by a collection of integer values on a second two dimensional lattice ($\Lambda_2 \subset \mathbb{Z}^2$, with the same dimensions as the CPM lattice), which remain constant for the duration of one season (τ_s MCS). The amount of chemotactic signal χ is largest at the peak, which is located at the center of one of the lattice boundaries, and from there decays linearly in all directions, forming a gradient: $\chi(d) = 1 + (k_\chi \frac{d_{\text{max}}}{100}) * (1 - \frac{d}{d_{\text{max}}})$, where k_χ is a scaling constant, d is the Euclidean distance of a lattice site from the peak of the gradient, and d_{max} is the maximum distance between the source of the gradient and any lattice site in Λ_2. Non integer values of χ are changed to $\lceil \chi \rceil$ (the smallest integer larger than χ) with probability equal to $\lceil \chi \rceil - \chi$, otherwise they are truncated to $\lfloor \chi \rfloor$ (the largest integer smaller than χ).

A cell s only perceives the chemotactic signal on the portion of Λ_2 corresponding to sites on Λ_1 with that spin. We define the vector $\vec{\chi}(c)$ as the vector that spans from the cell's center of mass to the center of mass of the perceived gradient. Copies of lattice sites are favoured when they align with the direction of the vector $\vec{\chi}(c)$, i.e. when there is a small angle θ_c between $\vec{\chi}(c)$ and the vector that spans from the center of mass of the cell to the lattice site into which copying is attempted (Fig. 1):

$$Y_{\text{chemotaxis}} = -\mu_\chi \cos(\theta_c)$$

where μ_χ is the maximal propensity to move along the perceived gradient, and is set to $\mu_\chi = 1$ except for dividing cells, whose $\mu_\chi = 0$. A uniform random $\theta_c \in [0, 2\pi[$ is chosen whenever

$|\vec{\chi}(c)| = 0$, i.e. when, locally, there is no gradient (due to the chemoattractant amount at each lattice site being rounded to integer values).

Seasonal dynamics A population of N cells undergoes the cell dynamics described above for the duration of a season, i.e. τ_s MCS. Cells can divide throughout the season, and upon division will pass on their regulatory network to the daughter cell with the possibility of mutations (described above). At the end of the season, we assess the distance of each cell from the peak of the chemokine gradient. The further the cell, the higher its probability of being killed before the new season starts. This is implemented as:

$$P_{\text{death}}(d_c) = p_{\text{min}} + \frac{(p_{\text{max}} - p_{\text{min}}) * d_c^3}{d_{\text{scale}}^3 + d_c^3}$$

where p_{min} is the minimum probability of dying, p_{max} the maximum probability, d_c is the distance of cell c to the peak of the gradient, and d_{scale} is the distance at which the death probability is at half of the maximum. The smaller d_{scale}, the more cells will die.

Table 2: Parameters

Parameter	explanation	Values
L^2	lattice size	500×500 lattice sites
T	Boltzmann temperature	16 AUE
λ	cell stiffness	4.0 AUE/[lattice site]^2
A_T	cell targetarea	50 lattice sites
Cell adhesion		
J_α	minimum J value between cells	4 AUE/[lattice site length]
J'_α	minimum J value between cell and medium	8 AUE/[lattice site length]
ν	length of receptor and ligand bitstring	24 bits
ν'	length ligand bitstring for medium adhesion	6 bits
Cell migration and chemotaxis		
μ_p	strength of persistent migration	3.0 AUE
τ_p	duration of persistence vector	50 MCS
μ_χ	strength of chemotaxis	1.0 AUE
k_χ	scaling factor chemoattractant gradient	5.0 molecules/[lattice site length]
Cell division		
η_{init}	time before cell in GRN state 1 can start growing	10000 MCS
η_{grow}	time for cell in state 1 to grow to 2x A_T and divide	20000 MCS
Evolution		
τ_s	duration of season	18×10^4 - 50×10^4 MCS
p_{min}	minimum probability of dying	0.05
p_{max}	maximum probability of dying	1.0
d_{scale}	distance from gradient peak where death probability is $\frac{1}{2}$ maximum	40 or 80 [lattice site length]
$\mu_{R,I}$	receptor and ligand mutation probability	0.01 per bit, per replication
μ_ω	mutation probability of network parameters (w, f, r_a)	0.02 per parameter, per replication
σ	standard deviation of mutation size	0.05

AUE: Arbitrary Units of Energy (see Hamiltonian in Model Section); lattice site: unit of area; lattice site length: unit of distance; MCS: Monte Carlo Step (unit of time).

References

[1] John Maynard Smith and Eors Szathmary. *The major transitions in evolution*. Oxford, UK: WE Freeman, 1995.

[2] Richard K Grosberg and Richard R Strathmann. The evolution of multicellularity: a minor major transition? *Annu. Rev. Ecol. Evol. Syst.*, 38:621–654, 2007.

[3] Thibaut Brunet and Nicole King. The origin of animal multicellularity and cell differentiation. *Developmental cell*, 43(2):124–140, 2017.

[4] Andrew H Knoll. The multiple origins of complex multicellularity. *Annual Review of Earth and Planetary Sciences*, 39:217–239, 2011.

[5] Martin E Boraas, Dianne B Seale, and Joseph E Boxhorn. Phagotrophy by a flagellate selects for colonial prey: a possible origin of multicellularity. *Evolutionary Ecology*, 12 (2):153–164, 1998.

[6] William C Ratcliff, R Ford Denison, Mark Borrello, and Michael Travisano. Experimental evolution of multicellularity. *Proceedings of the National Academy of Sciences*, 109(5): 1595–1600, 2012.

[7] Nicole King. The unicellular ancestry of animal development. *Developmental Cell*, 7(3): 313 – 325, 2004. ISSN 1534-5807.

[8] Stephen R. Fairclough, Zehua Chen, Eric Kramer, Qiandong Zeng, Sarah Young, Hugh M. Robertson, Emina Begovic, Daniel J. Richter, Carsten Russ, M. Jody Westbrook, Gerard Manning, B. Franz Lang, Brian Haas, Chad Nusbaum, and Nicole King. Premetazoan genome evolution and the regulation of cell differentiation in the choanoflagellate Salpingoeca rosetta. *Genome Biology*, 14(2):R15, February 2013. ISSN 1474-760X. doi: 10.1186/gb-2013-14-2-r15.

[9] Qingyou Du, Yoshinori Kawabe, Christina Schilde, Zhi-hui Chen, and Pauline Schaap. The evolution of aggregative multicellularity and cell–cell communication in the dictyostelia. *Journal of molecular biology*, 427(23):3722–3733, 2015.

[10] Núria Ros-Rocher, Alberto Pérez-Posada, Michelle M Leger, and Iñaki Ruiz-Trillo. The origin of animals: an ancestral reconstruction of the unicellular-to-multicellular transition. *Open Biology*, 11(2):200359, 2021.

[11] Antonis Rokas. The molecular origins of multicellular transitions. *Current opinion in genetics & development*, 18(6):472–478, 2008.

[12] Simon E Prochnik, James Umen, Aurora M Nedelcu, Armin Hallmann, Stephen M Miller, Ichiro Nishii, Patrick Ferris, Alan Kuo, Therese Mitros, Lillian K Fritz-Laylin, et al. Genomic analysis of organismal complexity in the multicellular green alga volvox carteri. *Science*, 329(5988):223–226, 2010.

[13] Daniel J Richter, Parinaz Fozouni, Michael B Eisen, and Nicole King. Gene family innovation, conservation and loss on the animal stem lineage. *Elife*, 7:e34226, 2018.

[14] Douglas H. Erwin. The origin of animal body plans: a view from fossil evidence and the regulatory genome. *Development*, 147(4), February 2020. ISSN 0950-1991, 1477-9129. doi: 10.1242/dev.182899.

[15] David L Kirk. A twelve-step program for evolving multicellularity and a division of labor. *BioEssays*, 27(3):299–310, 2005.

[16] Scott D Evans, Mary L Droser, and Douglas H Erwin. Developmental processes in ediacara macrofossils. *Proceedings of the Royal Society B*, 288(1945):20203055, 2021.

[17] Iaroslav Ispolatov, Martin Ackermann, and Michael Doebeli. Division of labour and the evolution of multicellularity. *Proceedings of the Royal Society B: Biological Sciences*, 279 (1734):1768–1776, 2011.

[18] Cristian A. Solari, John O. Kessler, and Raymond E. Goldstein. A general allometric and life-history model for cellular differentiation in the transition to multicellularity. *The American Naturalist*, 181(3):369–380, 2013. doi: 10.1086/669151. PMID: 23448886.

[19] Denis Tverskoi, Vladimir Makarenkov, and Fuad Aleskerov. Modeling functional specialization of a cell colony under different fecundity and viability rates and resource constraint. *PLOS ONE*, 13(8):1–27, 08 2018. doi: 10.1371/journal.pone.0201446.

[20] André Amado, Carlos Batista, and Paulo R.A. Campos. A mechanistic model for the evolution of multicellularity. *Physica A: Statistical Mechanics and its Applications*, 492: 1543–1554, 2018. ISSN 0378-4371. doi: https://doi.org/10.1016/j.physa.2017.11.080.

[21] Leonardo Miele and Silvia De Monte. Aggregative cycles evolve as a solution to conflicts in social investment. *PLoS computational biology*, 17(1):e1008617, 2021.

[22] Merlijn Staps, Jordi van Gestel, and Corina E Tarnita. Emergence of diverse life cycles and life histories at the origin of multicellularity. *Nature ecology & evolution*, 3(8):1197–1205, 2019.

[23] Salva Duran-Nebreda, Adriano Bonforti, Raúl Montanez, Sergi Valverde, and Ricard Solé. Emergence of proto-organisms from bistable stochastic differentiation and adhesion. *Journal of The Royal Society Interface*, 13(117):20160108, 2016.

[24] ES Colizzi, B van Dijk, RMH Merks, DE Rozen, and RMA Vroomans. Evolution of genome fragility enables microbial division of labor. *bioRxiv*, 2021.

[25] Chikara Furusawa and Kunihiko Kaneko. Origin of multicellular organisms as an inevitable consequence of dynamical systems. *The Anatomical Record*, 268(3):327–342, 2002.

[26] Paulien Hogeweg. Evolving mechanisms of morphogenesis: on the interplay between differential adhesion and cell differentiation. *Journal of Theoretical Biology*, 203(4):317 – 333, 2000. ISSN 0022-5193.

[27] Enrico Sandro Colizzi, Renske MA Vroomans, and Roeland MH Merks. Evolution of multicellularity by collective integration of spatial information. *eLife*, 9, 2020. doi: 10.7554/eLife.56349.

[28] François Graner and James A. Glazier. Simulation of biological cell sorting using a two-dimensional extended potts model. *Phys. Rev. Lett.*, 69:2013–2016, Sep 1992.

[29] James A. Glazier and François Graner. Simulation of the differential adhesion driven rearrangement of biological cells. *Phys. Rev. E*, 47:2128–2154, Mar 1993. doi: 10.1103/PhysRevE.47.2128.

[30] Josephine T. Daub and Roeland M. H. Merks. *Cell-Based Computational Modeling of Vascular Morphogenesis Using Tissue Simulation Toolkit*, pages 67–127. Springer New York, New York, NY, 2015. ISBN 978-1-4939-1462-3.

[31] Jordi van Gestel and Franz J. Weissing. Regulatory mechanisms link phenotypic plasticity to evolvability. *Scientific Reports*, 6(1):24524, Apr 2016. ISSN 2045-2322. doi: 10.1038/srep24524.

[32] Mark Zajac, Gerald L Jones, and James A Glazier. Simulating convergent extension by way of anisotropic differential adhesion. *Journal of Theoretical Biology*, 222(2):247–259, 2003.

[33] Renske MA Vroomans, Paulien Hogeweg, and Kirsten HWJ ten Tusscher. Segment-specific adhesion as a driver of convergent extension. *PLoS computational biology*, 11 (2):e1004092, 2015.

[34] Gavriel Matt and James Umen. Volvox: A simple algal model for embryogenesis, morphogenesis and cellular differentiation. *Developmental Biology*, 419(1):99–113, November 2016. doi: 10.1016/j.ydbio.2016.07.014. URL `https://doi.org/10.1016/j.ydbio.2016.07.014`.

[35] Pauline Schaap. Evolutionary crossroads in developmental biology: Dictyostelium discoideum. *Development*, 138(3):387–396, 2011.

[36] Lana Strmecki, David M. Greene, and Catherine J. Pears. Developmental decisions in dictyostelium discoideum. *Developmental Biology*, 284(1):25–36, 2005. ISSN 0012-1606. doi: https://doi.org/10.1016/j.ydbio.2005.05.011.

[37] Arielle Woznica, Alexandra M Cantley, Christine Beemelmanns, Elizaveta Freinkman, Jon Clardy, and Nicole King. Bacterial lipids activate, synergize, and inhibit a developmental switch in choanoflagellates. *Proceedings of the National Academy of Sciences*, 113 (28):7894–7899, 2016.

[38] José Muñoz-Dorado, Francisco J Marcos-Torres, Elena García-Bravo, Aurelio Moraleda-Muñoz, and Juana Pérez. Myxobacteria: moving, killing, feeding, and surviving together. *Frontiers in microbiology*, 7:781, 2016.

[39] Christopher Toret, Andrea Picco, Micaela Boiero-Sanders, Alphee Michelot, and Marko Kaksonen. The cellular slime mold fonticula alba forms a dynamic, multicellular collective while feeding on bacteria. *Current Biology*, 2022.

[40] Thomas Garcia, Leonardo Gregory Brunnet, and Silvia De Monte. Differential adhesion between moving particles as a mechanism for the evolution of social groups. *PLoS computational biology*, 10(2):e1003482, 2014.

[41] Jaideep Joshi, Iain D Couzin, Simon A Levin, and Vishwesha Guttal. Mobility can promote the evolution of cooperation via emergent self-assortment dynamics. *PLoS computational biology*, 13(9):e1005732, 2017.

[42] Kirill V. Mikhailov, Anastasiya V. Konstantinova, Mikhail A. Nikitin, Peter V. Troshin, Leonid Yu. Rusin, Vassily A. Lyubetsky, Yuri V. Panchin, Alexander P. Mylnikov, Leonid L. Moroz, Sudhir Kumar, and Vladimir V. Aleoshin. The origin of metazoa: a transition from temporal to spatial cell differentiation. *BioEssays*, 31(7):758–768, 2009. doi: https://doi.org/10.1002/bies.200800214.

[43] Renske MA Vroomans and Enrico Sandro Colizzi. cellevol 2.0: Tsto-based software and scripts for studying the evolution of differentiated multicellularity. 2022. URL `https://github.com/RenskeVroomans/regulation_evolution`.

[44] James A Glazier, Ariel Balter, and Nikodem J Popławski. Magnetization to morphogenesis: a brief history of the glazier-graner-hogeweg model. In *Single-Cell-Based Models in Biology and Medicine*, pages 79–106. Springer, 2007.

[45] Joost B. Beltman, Athanasius F.M. Marée, Jennifer N. Lynch, Mark J. Miller, and Rob J. de Boer. Lymph node topology dictates T cell migration behavior . *The Journal of Experimental Medicine*, 204(4):771–780, 03 2007. ISSN 0022-1007.

Supplementary material

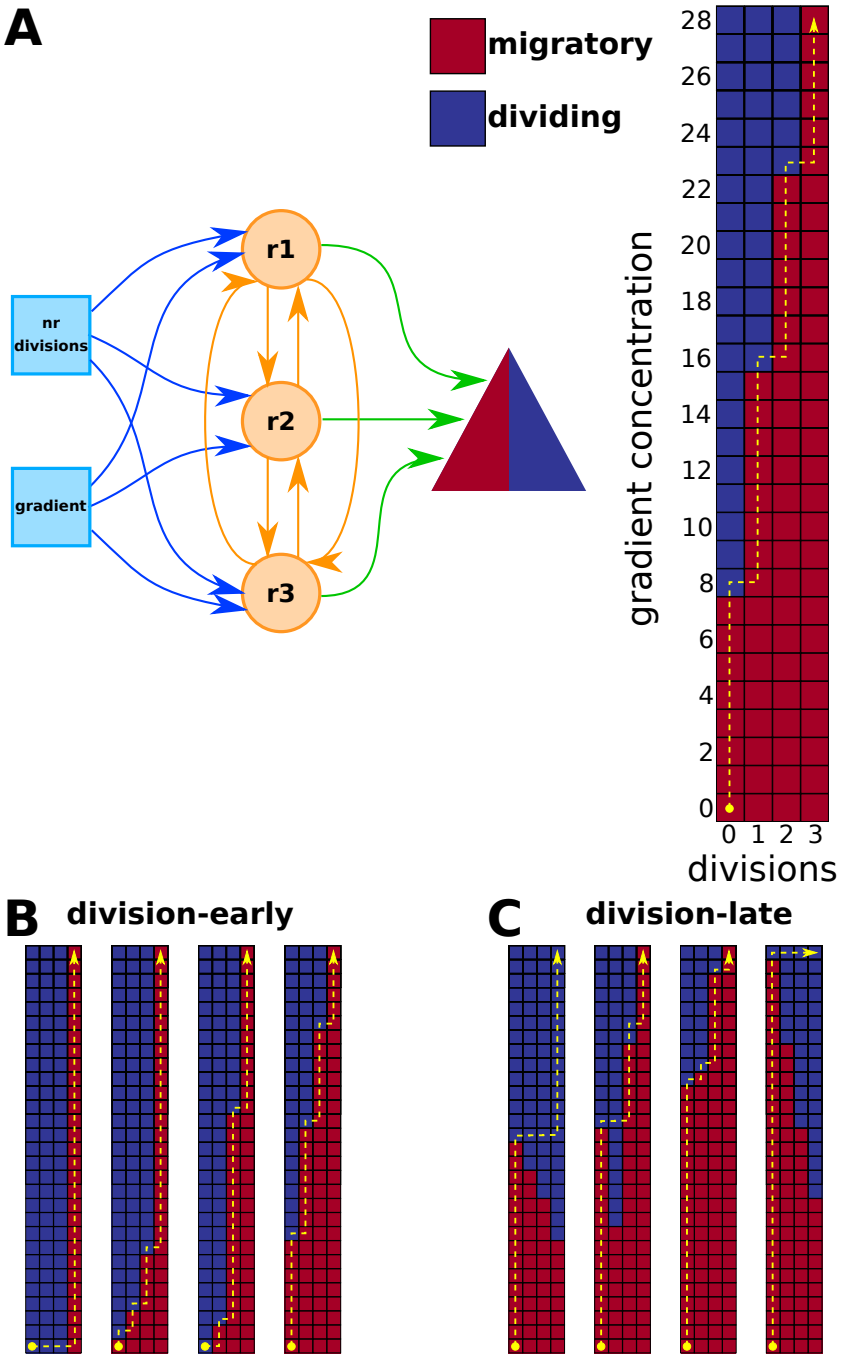

Figure S1: Assessment of evolved GRN responses in unicellular simulations

A) We assess the steady state of the output node for all combinations of values for the input nodes (gradient concentration and number of divisions) that are possible in the simulation (with the other nodes starting at 0), and then assign that combination a color in the 2D profile, with red=migratory (output node 0), blue=dividing (output node 1). The profile can be read by starting on the bottom-left, moving up when the pixel is red (migrating to higher concentration), and right when it is blue (dividing and increasing the number of divisions the cell has done).

B) Examples of GRN responses of division-early, mixed, and division-late strategies. These have then been used for the simulations with harsher conditions.

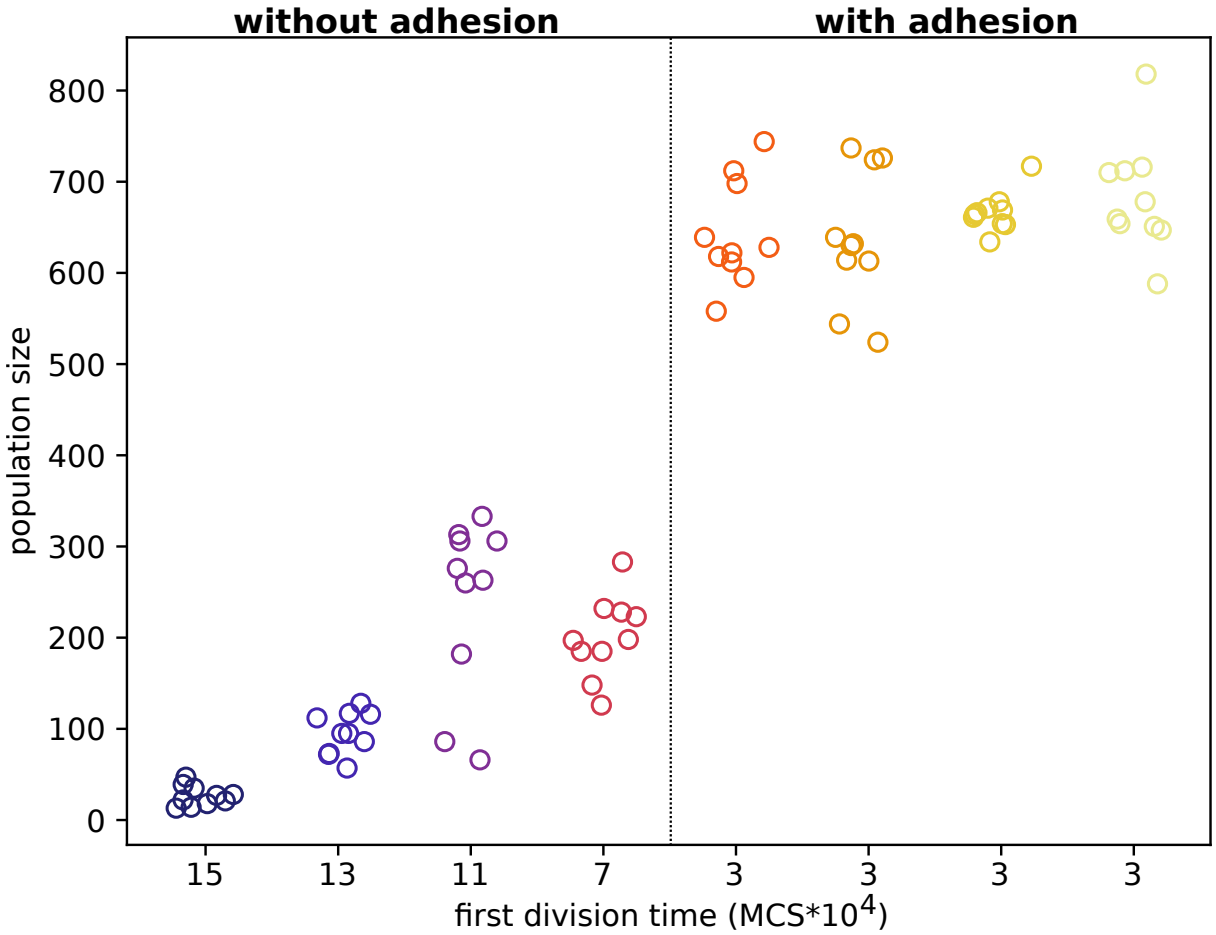

Figure S2: Evolved population size

The population sizes at the end of the last ten seasons in simulations with high death rate and very short seasons. Simulations are sorted by their median first division times (indicated on the x axis), from the simulations that were then used to pick ancestors for the switched simulations. Colours group data from the same simulation. Resolution on division timing was limited to 10000 MCS.

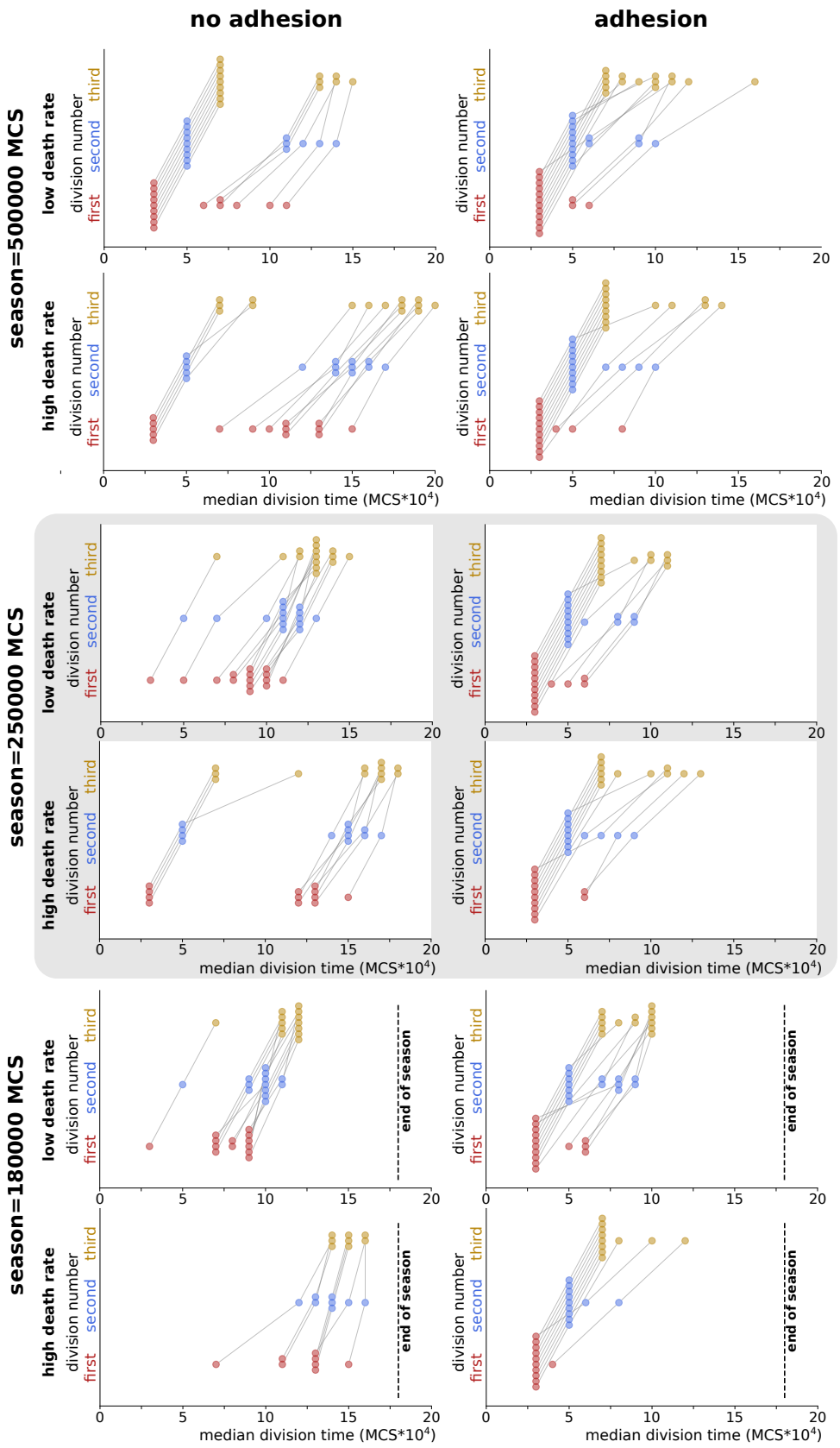

Figure S3: Evolved division timing strategies in all simulation sets

The median timing of cell divisions of the last 10 seasons in all sets of simulations, with varying season duration, death rates and with or without evolution of adhesion. Lines between dots connect values belonging to the same simulations.

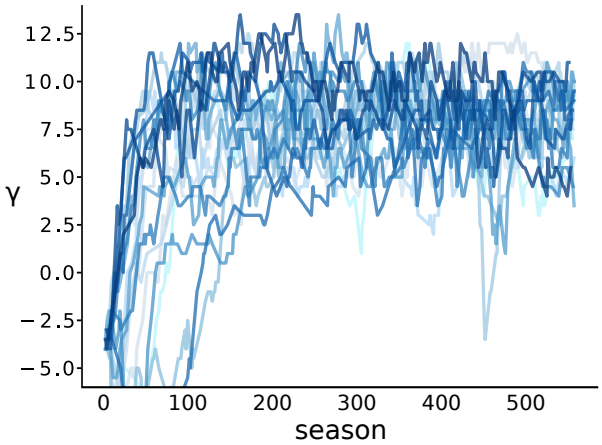

Figure S4: Evolution of adhesion in simulations starting from indivual evolved without adhesion
Evolution of adhesion in 20 simulations, started with 4 individuals that had evolved without adhesion (5 independent simulations per individual)

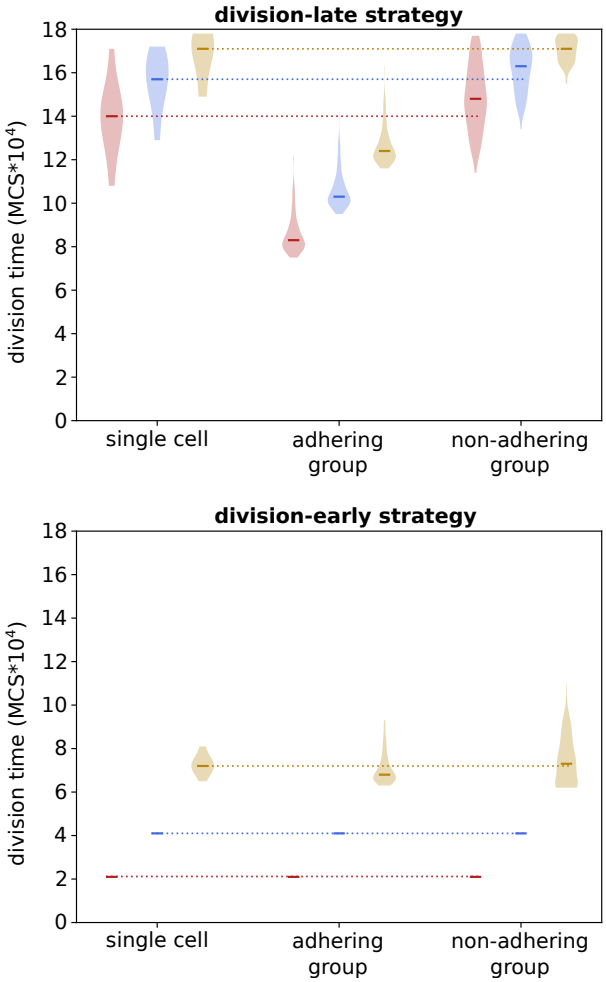

Figure S5: Effect of adhesion or non-adhesion on division timing

The distribution of division timings for simulations with a single cell compared to simulations of one season with 20 adhering or non-adhering cells. For simplicity, divisions were simulated by giving the cell the dividing state for the same amount of time, but no additional daughter cell was created. This kept the group size the same throughout the run. There were also no mutations of adhesion or regulation. We show here two example genomes, one evolved without adhesion, possessing a division-late strategy; and one evolved with adhesion, possessing a division-early strategy. Season duration=180000.

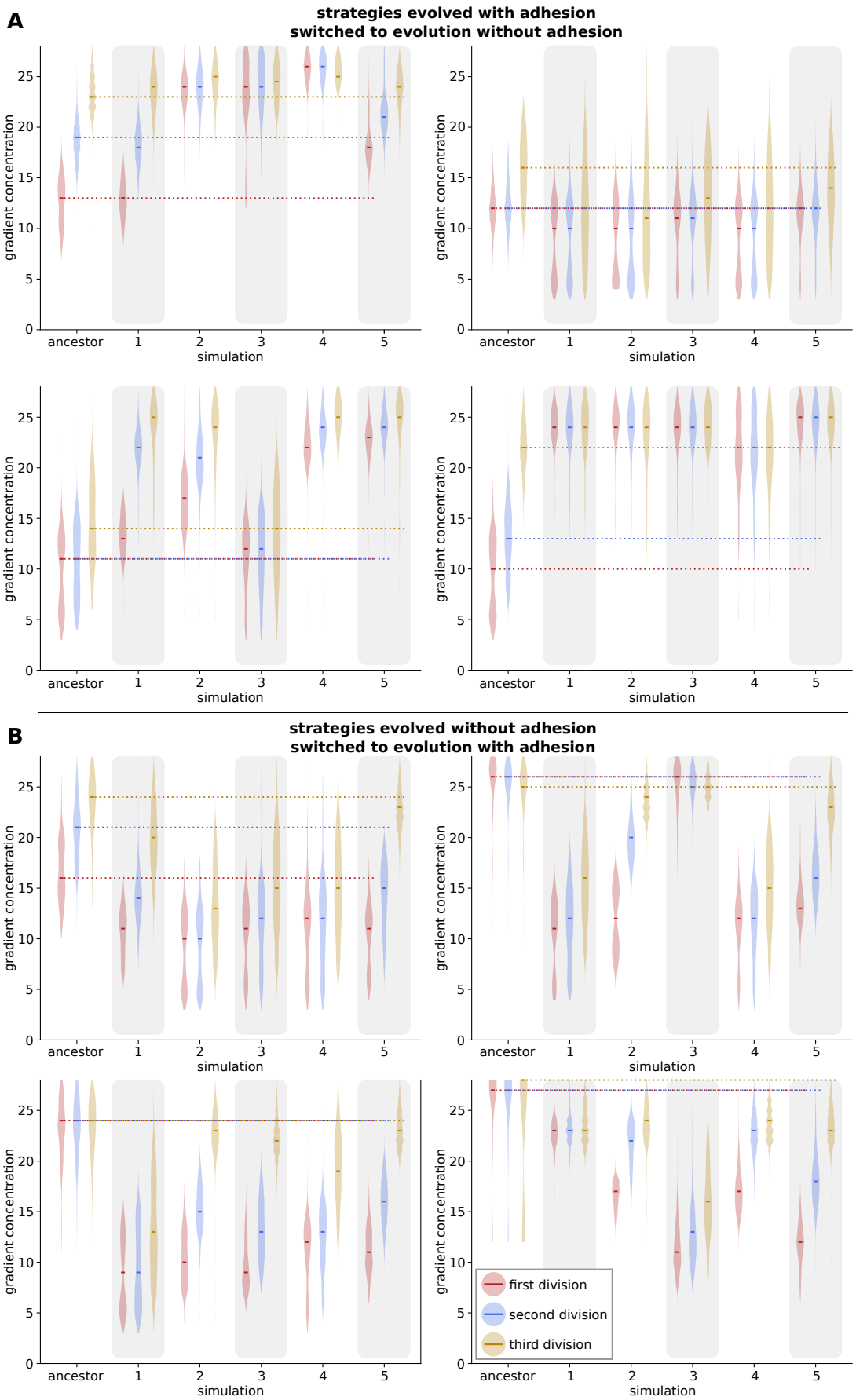

Figure S6: Evolution of gradient sensing after adhesion switch

Shown are the population distributions of the gradient level at which a division happens, before the switch in adhesion (ancestor) and the five replicate simulations evolved from that ancestor after the switch.

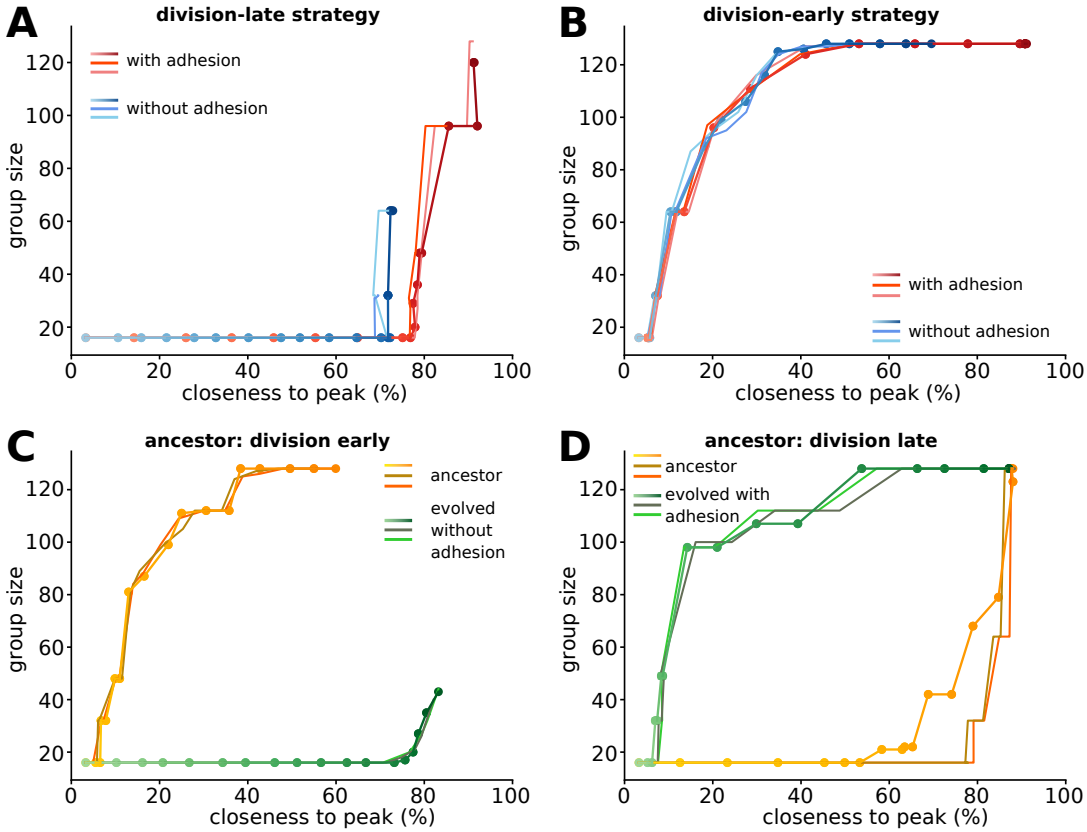

Figure S7: Replicates of competition experiment

Group size plotted against the median distance of cells to the peak of gradient, shown for the first season of the competition experiment (0%=maximum distance, 100%=at the peak). The graded lines with dots are the same as in figure 5. **a-b)** Competition between two groups with the same regulatory strategy, one adhering ($\gamma = 6$; a), the other non-adhering ($\gamma = -4$; b). **c)** Competition between ancestral, division-early strategy and evolved, division-late strategy; both non-adhering. **d)** Competition between two adhering groups, one with an ancestral, division-late strategy and one with a strategy evolved after 500 seasons with possibility of adhesion (having become more division-early).

Supplementary Videos

1. One season of a simulation which evolved a division-early strategy (Season duration=250000; high death rate; adhesion cannot evolve)

2. One season of a simulation which evolved a division-early strategy (Season duration=250000; high death rate; adhesion can evolve).

3. One season of a simulation which evolved a division-late strategy (Season duration=250000; high death rate; adhesion cannot evolve)

4. One season of a simulation which evolved a division-late strategy (Season duration=250000; high death rate; adhesion can evolve).

5. A competition experiment between a cluster of adhering cells and a cluster of non-adhering cells, with division-late strategy.

6. A competition experiment between a cluster of adhering cells and a cluster of non-adhering cells, with division-early strategy.

7. A competition experiment between a cluster of division-early ancestors and a cluster of division-late descendants – both nonadhering.

8. A competition experiment between a cluster of division-late ancestors and a cluster of division-early descendants – both adhering.

9. One season of a simulation with a clonal cluster of initially 50 cells (i.e. all have the same regulatory strategy). Individual regulatory strategy taken from the last season of a simulation in which the population was switched from non-adhering to evolution of adhesion.